Efficient Resonance Mode Analysis-Based Methodology for Resonance Studies in Multi-Terminal Transmission Grids

Oriol Cartiel, Juan José Mesas, and Luis Sainz

***Abstract*—Resonances in transmission grids can increase harmonic voltages and currents in the presence of nonlinear loads and cause dynamic instabilities. Although frequency scan analysis is commonly used to assess resonances, resonance mode analysis (RMA) provides a more detailed understanding of resonances and is more useful for harmonic power quality and stability studies. However, RMA is a time-consuming task that involves eigenpair decomposition of the impedance matrix over a frequency range. To reduce computational effort, rapid RMA (r_RMA) based on the power iteration method, or faster RMA (f_RMA), are proposed, but these approaches can suffer from convergence issues due to the matrix spectrum. To amend this, the paper contributes a Lanczos method-based RMA (L_RMA) that applies the non-Hermitian Lanczos method to obtain the dominant eigenvalue of the impedance matrix. The accuracies, computational times and convergence rates of the four RMA-based approaches (RMA, r_RMA, f_RMA and L_RMA) are compared in ten IEEE and seven synthetic test power systems. It is verified that r_RMA and f_RMA are the best choices for small transmission grids, while L_RMA offers significant time-saving benefits in large multi-terminal transmission grids with sparse admittance matrices. Overall, the study offers an RMA-based methodology for resonance studies validated by MATLAB/Simulink simulation.**

***Index Terms*—Resonance, modal analysis, power iteration, Krylov subspace, Lanczos method, sparse matrix.**

I. Introduction

RESONANCES in transmission grids have recently become a major concern due to the growing presence of electronic devices. Peak values of grid impedances at resonance frequencies can increase the harmonic currents consumed by these devices, worsening voltage and harmonic current distortion [1]. Low damped resonances can also cause voltage oscillatory instabilities at resonance frequencies [2]. These resonances are characterised by the non-Hermitian admittance matrices of transmission grids, and the frequency scan analysis applied to the inverse of these matrices (i.e., to the impedance matrix) is probably the most common tool employed by engineers to calculate resonance frequencies [1], [3]. With this frequency domain approach, it is also possible to deal with black-box models of transmission grid components that cannot be further identified by white-box models. The integration of black-box models into the admittance matrix for frequency scan analysis of resonances is currently a key focus in harmonic and stability studies [4]. Nevertheless, frequency scan analysis has several drawbacks, such as high computational effort to study the sizeable admittance matrices of large multi-terminal transmission grids.

Resonance mode analysis (RMA) enhances the study of resonances through eigenvalue analysis of the admittance/impedance matrix [3]. This analysis is particularly interesting in engineering because the study of complex coupled systems, such as transmission grids, can be simplified to scalar multiplications. Moreover, eigenvalue analysis can provide useful insights into the system's behaviour. In particular, RMA solves not only the resonance frequency characterisation but also other concerns related to the above resonances (e.g., finding the best grid location to damp resonances and the grid components involved in them) [3], [5], [6]. Currently, RMA is applied to harmonic power quality studies and some impedance-based approaches for stability assessment of multi-terminal hybrid AC/DC transmission grids [4], [7], [8], [9], [10].

As previously mentioned, RMA is a useful tool for stability and harmonic analysis, but requires a high computational effort to calculate the eigenvalue decomposition of the impedance matrix over the whole frequency range, that can increase dramatically in large multi-terminal transmission grids. There are different methods for solving eigenproblems that can be divided into direct and iterative methods [11], [12], [13]. Iterative methods are the most appropriate for determining eigenvalues of large, sparse matrices, such as the admittance matrices of large multi-terminal transmission grids. These methods can be grouped under those that are applicable to Hermitian matrices and those that are applicable to non-Hermitian matrices. The latter are of interest for this study because of the nature of the aforementioned admittance matrices.

Single- and multi-vector iteration methods, such as the power iteration (PI)-based method, are the simplest iterative algorithms for computing the dominant eigenvalue of any eigenproblem. Accordingly, a rapid RMA (r_RMA) approach based on the

Received 23 November 2023; revised 18 May 2024 and 19 September 2024; accepted 3 November 2024. Date of publication 7 November 2024; date of current version 24 January 2025. This work was supported in part by MICIU/AEI/10.13039/501100011033 and in part by European Union Next Generation EU/PRTR under Grant TED2021-129631B-C33. Paper no. TPWRD-01640-2023. *(Corresponding author: Juan José Mesas.)*

Oriol Cartiel and Luis Sainz are with the Department of Electrical Engineering, ETSEIB, UPC, 08028 Barcelona, Spain (e-mail: oriol.cartiel@upc.edu; luis.sainz@upc.edu).

Juan José Mesas is with the Department of Electrical Engineering, EEBE, UPC, 08019 Barcelona, Spain (e-mail: juan.jose.mesas@upc.edu).

Color versions of one or more figures in this article are available at https://doi.org/10.1109/TPWRD.2024.3493381.

Digital Object Identifier 10.1109/TPWRD.2024.3493381

PI method is presented in [14] and [15], and a faster RMA (f_RMA) approach in [16]. Given an eigenproblem $\mathbf{Ax} = \lambda \mathbf{x}$ with a matrix $\mathbf{A} \in C^{nxn}$, the PI method generates a sequence of vectors $\mathbf{x}_1, \ldots, \mathbf{x}_k$ that span a *Krylov subspace* $\mathcal{K}_k(\mathbf{A}, \mathbf{x}_1, k) = span\{\mathbf{x}_1, \mathbf{Ax}_1, \ldots, \mathbf{A}^{k-1}\mathbf{x}_1\}$ such that the vector $\mathbf{x}_k$ converges to the dominant right eigenvector of $\mathbf{A}$ after several iterations [11], [12], [13]. The PI method is a computationally efficient tool as it calculates only the dominant eigenvalue of the impedance matrix at each frequency. However, convergence heavily depends on the matrix spectrum, potentially leading to slow or incomplete convergence [11], [12], [13]. The Arnoldi method and the non-Hermitian Lanczos method are the most efficient iterative algorithms for large, sparse, non-Hermitian matrices [17], [18], [19], [20], [21]. These methods can effectively overcome the convergence issues of the PI method and solve large, sparse matrix eigenproblems [12], [13], [17], [18], [19], [20], [21], [22], [23], [24], [25], [26]. They are commonly used to solve large-dimensional matrix equations in engineering eigenvalue problems (e.g., in structural analysis, control theory, image and signal processing, and machine learning). However, to the best of the authors' knowledge, they have not yet been applied to resonance studies in transmission grids. The Arnoldi method is an orthogonal projection algorithm that leads to a sequence of Hessenberg matrices $\mathbf{H}_k$ resulting from the application of the orthogonal vectors of the Krylov matrix $\mathbf{K}_k(\mathbf{A}, \mathbf{x}_1, k) = [\mathbf{q}_1, \mathbf{Aq}_1, \ldots, \mathbf{A}^{k-1}\mathbf{q}_1]$. The non-Hermitian Lanczos method is an oblique projection algorithm that yields a sequence of tridiagonal matrices $\mathbf{T}_k$ resulting from the application of the biorthogonal vectors of the Krylov matrices $\mathbf{K}_k(\mathbf{A}, \mathbf{x}_1, k) = [\mathbf{x}_1, \mathbf{Ax}_1, \ldots, \mathbf{A}^{k-1}\mathbf{x}_1] (\mathbf{x}_1 = \mathbf{q}_1$ and $\mathbf{p}_1)$. The above Arnoldi and Lanczos vectors are applied to matrix $\mathbf{A}$, and the extreme modulus eigenvalues of $\mathbf{H}_k$ and $\mathbf{T}_k$ (known as Ritz values) progressively provide better estimates of the extreme modulus eigenvalues of $\mathbf{A}$ [13], [17], [18], [22]. It should be noted that, at any iteration k, the PI method estimates the dominant eigenvalue of $\mathbf{A}$ in the subspace generated by the vector $\mathbf{x}_k = \mathbf{A}^{k-1}\mathbf{x}_1$, while the Arnoldi and non-Hermitian Lanczos methods do so by taking all vectors $\mathbf{x}_1, \mathbf{Ax}_1, \ldots, \mathbf{A}^{k-1}\mathbf{x}_1$ of the Krylov matrices. This consideration leads to better and more efficient approximations of the dominant eigenvalue, since the Krylov matrices contain all the information of the generated subspace [13], [17], [20]. The most popular Krylov subspace method for non-Hermitian matrices is the Arnoldi algorithm [18]. Several studies compare the Arnoldi method with the non-Hermitian Lanczos method [13], [17], [18], [19], [20], [21], [23], and none of them clearly favours one over the other. In any case, the Lanczos method offers several advantages over the Arnoldi method [18], [19], [20], [21].

The increasing presence of power electronics and HVDC links in transmission grids makes it necessary to efficiently perform RMA in resulting large multi-terminal transmission grids, including the so-called super grids [24], [25]. The admittance matrices of these grids are logically large and, in most cases, sparse. Under these circumstances, the computational effort and time of any RMA performed with any of the existing RMA approaches are unacceptable regardless of how often RMA is performed, not to mention the inability of these approaches to directly obtain the left eigenvectors of the admittance/impedance matrices over the entire frequency range. Therefore, an efficient RMA-based methodology is needed to overcome the above limitations in large multi-terminal transmission grid resonance studies, which seem to be increasingly common.

This paper presents a novel, original and relevant contribution to the engineering problem of studying resonances in multi-terminal transmission grids through an RMA-based methodology that integrates black-box models. The contributed methodology adequately combines two RMA approaches: an existing one, the r_RMA (or f_RMA) approach, which is more efficient in small transmission grids, and a new one proposed by the authors, the non-Hermitian Lanczos method-based RMA (L_RMA) approach, which is more efficient in large multi-terminal transmission grids with highly sparse admittance matrices. This methodology considers the sparsity ratio of the admittance matrix [27], [28], [29], [30] to apply r_RMA (or f_RMA) or L_RMA. L_RMA is a novel RMA-based approach that applies the non-Hermitian Lanczos method to efficiently obtain the dominant eigenvalue of the impedance matrix with its corresponding left and right eigenvectors in large multi-terminal transmission grids over the entire frequency range.

If this RMA-based methodology is intended to be used appropriately for resonance studies in multi-terminal transmission grids, it is essential to know the basics of the two RMA approaches it combines, understand the advantages of these two RMA approaches over other existing or possible RMA approaches, and analyse the application of the resulting methodology for resonance studies to be performed efficiently regardless the size of the multi-terminal transmission grid. The study is presented with mathematical rigour and includes extensive applications, the results of which are validated by MATLAB/Simulink (MATSIM) simulations, demonstrating the clear advantage of the L_RMA approach over other approaches for large-scale power systems. A comparative study of RMA, r_RMA, f_RMA, and L_RMA accuracies, computational times and convergence rates is performed on the IEEE 3– [31], 5– [32], 9– [33], 14– [34], 24– [35], 30– [36], 39– [37], 57– [38], 118– [39], and 300– [40] bus test power systems, as well as Central Illinois 200– [41], South Carolina 500– [42], Texas 2k– [43], Texas 7k– [44], East Coast USA 10k– [45], North Central USA 25k– [45] and Eastern USA 70k– [45] bus synthetic test power systems. In addition, small-signal *converter-driven stability* [46] is assessed in a modified IEEE 118–bus test power system using the positive-mode-damping (PMD) stability criterion [7].

The paper is organised as follows. Section II presents the limitations of frequency scan analysis in resonance studies and the basics of two existing RMA-based approaches, RMA and r_RMA, as well as a brief description of a third RMA-based approach, f_RMA. These approaches enhance resonance studies but they are computationally intensive when applied to large multi-terminal transmission grids. In Section III, the basics and the algorithm of the non-Hermitian Lanczos method are provided to reduce this computational effort, and its suitability for large, sparse eigenproblems is discussed. A new RMA-based approach, L_RMA, based on the non-Hermitian Lanczos method is developed in Section IV, which is logically

suitable for resonance studies in large multi-terminal transmission grids with sparse admittance matrices. For resonance studies to be performed efficiently regardless the size of the multi-terminal transmission grid, a novel RMA-based methodology is proposed in Section V. This technique applies the most efficient RMA-based approach while considering the sparsity ratio of the admittance matrix. The integration of black-box models in the methodology is also described. In Section VI, the proposed methodology is applied and some results are obtained as quantitative evidence of the efficiency of the L_RMA approach. Finally, Section VII draws conclusions from these results.

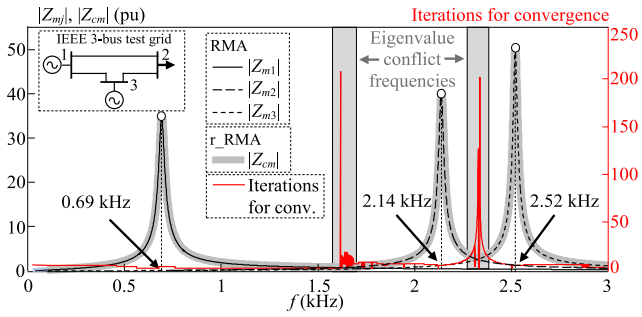

Fig. 1. RMA and r_RMA results in IEEE 3-bus test power system [31].

II. Resonance Mode Analysis

Frequency scan analysis is the traditional tool for determining resonance frequencies in harmonic power quality studies, but it does not provide all the required information for an effective resolution of the problem [1], [3]. This analysis is based on the voltage node method,

$$\mathbf{V}_{\mathbf{B},f} = \mathbf{Y}_{\mathbf{B},f}^{-1}\,\mathbf{I}_{\mathbf{B},f} = \mathbf{Z}_{\mathbf{B},f}\,\mathbf{I}_{\mathbf{B},f}, \tag{1}$$

where $\mathbf{V}_{\mathbf{B},f}$ is the voltage vector, $\mathbf{I}_{\mathbf{B},f}$ the current injection vector, $\mathbf{Y}_{\mathbf{B},f}$ the admittance matrix and $\mathbf{Z}_{\mathbf{B},f} = \mathbf{Y}_{\mathbf{B},f}^{-1}$ is the impedance matrix at frequency f.

The frequency behaviour of the $\mathbf{Z}_{\mathbf{B},f}$ terms (driving and coupling point impedances) characterises the frequency response of transmission grids, making it possible to investigate the frequencies of grid resonances (i.e., peak values of the $\mathbf{Z}_{\mathbf{B},f}$ components), which can cause high bus voltage values at these frequencies. These peak values define the resonance frequencies and are associated with singularities in the admittance matrix $\mathbf{Y}_{\mathbf{B},f}$.

However, the influence of grid buses on resonances cannot be characterised by this analysis. Moreover, the study of large transmission grids has a very high computational cost due to the high number of buses and impedances associated with the grid.

In order to overcome the limitations of frequency scan analysis, RMA is presented as a powerful tool to characterise resonance frequencies [3]. Nevertheless, RMA requires the eigenvalue decomposition of the admittance matrix at each frequency, which can be computationally intensive in large multi-terminal transmission grids. To reduce the computational time, an alternative PI method-based approach called r_RMA was developed [11], [14], [15].

A. Basics of the Resonance Mode Analysis

RMA is based on the eigenanalysis of the voltage node method (1) at each frequency f, i.e., [3]

$$\mathbf{V}_{\mathbf{B},f} = \mathbf{Y}_{\mathbf{B},f}^{-1}\,\mathbf{I}_{\mathbf{B},f} \;\rightarrow\; \mathbf{U}_f = \mathbf{\Lambda}_{\mathbf{Y},f}^{-1}\,\mathbf{J}_f$$

$$\mathbf{\Lambda}_{\mathbf{Y},f} = \begin{bmatrix} \lambda_{Y1} & & 0 \\ & \ddots & \\ 0 & & \lambda_{Yn} \end{bmatrix}_f = \mathbf{L}_f\,\mathbf{Y}_{\mathbf{B},f}\,\mathbf{R}_f, \tag{2}$$

where n is the number of the grid buses, $\mathbf{U}_f = \mathbf{L}_f\ \mathbf{V}_{\mathbf{B},f}$ and $\mathbf{J}_f = \mathbf{L}_f\ \mathbf{I}_{\mathbf{B},f}$ are the modal voltage and current vectors, respectively, $\mathbf{\Lambda}_{\mathbf{Y},f}$ is the eigenvalue matrix of $\mathbf{Y}_{\mathbf{B},f}$ and $\mathbf{R}_f = [\mathbf{R}_1\ \ \ldots\ \ \mathbf{R}_n]_f$ and $\mathbf{L}_f = [\mathbf{L}_1\ \ \ldots\ \ \mathbf{L}_n]_f^{\mathrm{T}}$ are the right (in columns) and left (in rows) eigenvector matrices, respectively, where $\mathbf{R}_f = \mathbf{L}_f^{-1} = \mathbf{L}_f^{\mathrm{T}}$ since $\mathbf{Y}_{\mathbf{B},f}$ is symmetric and non-Hermitian in all the studied cases of transmission grids.

Eigenvalues of the admittance matrix $\mathbf{Y}_{\mathbf{B},f}$ (see (2)) are all the modes of the transmission grid at each frequency, whereas resonance modes are only those eigenvalues whose moduli over a frequency range have local minima (i.e., singularities). These singularities coincide with peak values of the moduli of the impedance matrix eigenvalues $Z_{mj,f} = 1/\lambda_{Yj,f}$, known as resonance modal impedances. The resonance frequencies are the same as the frequencies at which the resonance modal impedances have these local extremes. At each frequency, the largest modulus eigenvalue of the impedance matrix is called the critical mode (or critical modal impedance). Thus, it can also be stated that the resonance frequencies coincide with the frequencies at which the critical mode has local modulus extremes.

RMA can also determine the relationship (excitability and observability) between the grid buses b and the critical resonance modes j using the participation factors (PFs), PF_{bj}, calculated with the right and left eigenvectors [3]. Moreover, the influence of grid elements on each critical resonance mode can be studied using the sensitivity matrix [5], [6].

Although RMA has significant advantages over frequency scan analysis, it also has a high computational cost due to the diagonalisation of the admittance matrix, which increases with the grid size.

B. Basics of the Rapid Resonance Mode Analysis

In order to determine resonance frequencies, RMA only requires to obtain the largest modulus eigenvalue (critical mode) of the impedance matrix at each frequency. Based on this, r_RMA only calculates this eigenvalue and its associated right eigenvector using the PI method [11], [14], [15]. Therefore, the result of applying r_RMA is the envelope of all the impedance matrix modes obtained by RMA [14], [15]. This can be observed in Fig. 1 for RMA and r_RMA studies of the IEEE 3−bus test power system [31].

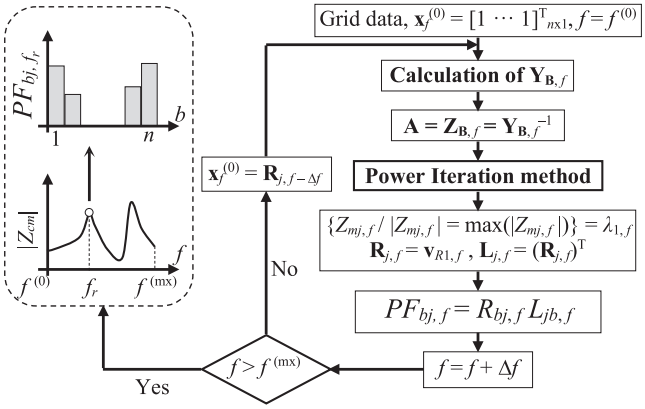

Fig. 2. Flowchart of r_RMA.

Power iteration (PI) method: Given a diagonalisable matrix $\mathbf{A} \in C^{nxn}$ with its eigenvalues λ_i such that $|\lambda_1| > \ldots \geq |\lambda_n|$ and its associated right unit eigenvectors $\mathbf{v}_{Ri}(i = 1, \ldots, n)$, the dominant eigenvalue λ_1 and its eigenvector $\mathbf{v}_{R1}$ can be obtained by the next iterative algorithm, which starts from an arbitrary initial vector $\mathbf{x}^{(0)}$ [11], [14], [15],

$$\mathbf{y}^{(k)} = \frac{\mathbf{x}^{(k)}}{\left|\left|\mathbf{x}^{(k)}\right|\right|_2}, \ \mathbf{x}^{(k+1)} = \mathbf{A}\mathbf{y}^{(k)}$$
$$\sigma^{(k)} = \mathbf{y}^{(k)\mathrm{T}}\mathbf{x}^{(k+1)} \ \ (k \geq 0), \tag{3}$$

where $\|\cdot\|_2$ represents the two-norm of a vector. The sequences $\mathbf{y}^{(k)}$ and $\sigma^{(k)}$ converge to $\mathbf{v}_{R1}$ and λ_1, respectively [14].

The convergence speed of the PI method depends essentially on the ratio $|\lambda_2/\lambda_1|$, where λ_1 and λ_2 are the two dominant eigenvalues (i.e., the largest modulus eigenvalues) of matrix $\mathbf{A}$. If $|\lambda_2/\lambda_1| \cong 0$, the iterative algorithm converges very fast whereas, if $|\lambda_2|$ is close to $|\lambda_1|$ ($|\lambda_2/\lambda_1| \cong 1$), the PI method may have convergence problems and even fail to converge [11], [14], [15]. A combination of a convergence rate (based on the eigenvalues or on the infinity-norm $\|\cdot\|_\infty$ of eigenvectors [15]) and a convergence acceleration is commonly applied as a stopping criterion for the PI algorithm, i.e.,

$$\varepsilon^{(k)} = \frac{\left|p^{(k)} - p^{(k-1)}\right|}{\left|p^{(k-1)}\right|} < \Delta \quad (p = \sigma \text{ or } ||\mathbf{x}||_\infty)$$
$$\xi^{(k)} = \left|\varepsilon^{(k)} - \varepsilon^{(k-1)}\right| < \delta. \tag{4}$$

Then, if $\varepsilon^{(k)}$ or $\xi^{(k)}$ falls below the established thresholds of Δ or δ (where $\Delta = 10^{-10}$ and $\delta = 10^{-6}$ are suggested), respectively, the PI algorithm stops.

Fig. 2 shows the complete r_RMA flowchart, which is based on the PI method with $\mathbf{A} = \mathbf{Z}_{\mathbf{B},f} = \mathbf{Y}_{\mathbf{B},f}^{-1}$. It must be noted that the convergence rate is strongly dependent on the starting vector of the PI method, and the eigenvector at the previous frequency becomes a good starting vector, i.e., $\mathbf{x}_{f\neq f^{(0)}} = \mathbf{R}_{j,\ f-\Delta f}$. The starting vector at the first frequency is chosen as $\mathbf{x}_{f^{(0)}} = [1 \cdots 1]^{\mathrm{T}}{}_{n\mathrm{x}1}$ [14], [15]. The PI method yields the largest modulus eigenvalue $Z_{mj,f}$ of the impedance matrix $\mathbf{Z}_{\mathbf{B},f}$ and its corresponding right unit eigenvector $\mathbf{R}_{j,f}$ over the whole frequency range. Hence, r_RMA allows the evolution envelope of the moduli of all modal impedances $Z_{mj,f}$ of $\mathbf{Z}_{\mathbf{B},f}$ over the entire frequency range (see Fig. 1) to be calculated, denoted by $|Z_{cm}|$, i.e.,

$$|Z_{cm}| = \left\{|Z_{mj,f} \mid / \ |Z_{mj,f}| = \max\left(|Z_{mj,f}|\right) \right.$$
$$\left. \forall f \in \left[f^{(0)}, f^{\,(mx)}\right]\right\}. \tag{5}$$

As can be observed in Fig. 1, the PI method has convergence problems indicated by a high number of iterations at *eigenvalue conflict frequencies*, where $\mathbf{Z}_{\mathbf{B},f}$ has two dominant eigenvalues (i.e., at frequencies where $|\lambda_1| \approx |\lambda_2|$). This is a major drawback in large multi-terminal transmission grids, and early stopping of the PI method by setting a maximum number of iterations for convergence (k_{conv}^{mx}) is therefore appropriate to prevent the PI method from continuing unnecessarily because there are no resonances at these frequencies.

A f_RMA approach based on a modified shifted-inverse power iteration method has recently been proposed. It is an improvement over the r_RMA approach to enhance its performance (see details in [16]).

III. Non-Hermitian Lanczos Method

Although r_RMA is a powerful tool based on the PI method to determine the largest modulus eigenvalue of an eigenproblem $\mathbf{Ax} = \lambda\mathbf{x}$ (e.g., the RMA eigenproblem, where $\mathbf{A} = \mathbf{Y}_{\mathbf{B},f}$ and the PI method is applied at each frequency f), it suffers from a severe convergence issue at the *eigenvalue conflict frequencies* that limits its usefulness in studying large multi-terminal transmission grids with a high number of eigenvalues [11]. To overcome the limitation, the paper presents L_RMA, a more suitable approach for large, sparse eigenproblems derived from the *Krylov subspaces* projection methods, in particular, the non-Hermitian Lanczos method [12], [13], [17], [18], [19], [20], [21]. The approach generates a sequence of tridiagonal matrices $\mathbf{T}_k$ whose extreme modulus eigenvalues are gradually better estimates of $\mathbf{A}$'s extreme modulus eigenvalues with a fast convergence rate.

A. Basics of the Non-Hermitian Lanczos Method

The following two theorems get closer to the non-Hermitian Lanczos method and L_RMA [13]:

Theorem 1: Given a non-Hermitian matrix $\mathbf{A} \in C^{nxn}$ and its eigenvalues $\lambda_i(i = 1, \ldots, n)$ with $|\lambda_1| > \ldots \geq |\lambda_n|$, there exist two biorthogonal matrices $\mathbf{P} = [\mathbf{p}_1, \ldots, \mathbf{p}_n]$ and $\mathbf{Q} = [\mathbf{q}_1, \ldots, \mathbf{q}_n](\mathbf{P}^{\mathrm{T}}\mathbf{Q} = \mathbf{I}_n)$ of vectors $\mathbf{p}_i$ and $\mathbf{q}_i \in C^n$ such that the extreme modulus eigenvalues of the matrix $\mathbf{P}^{\mathrm{T}}\mathbf{AQ}$ converge to λ_1 and λ_n [12].

Theorem 2: Given a non-Hermitian matrix $\mathbf{A} \in C^{nxn}$ and its eigenvalues $\lambda_i(i = 1, \ldots, n)$ with $|\lambda_1| > \ldots \geq |\lambda_n|$, the Rayleigh-Ritz procedure ensures that the extreme modulus eigenvalues μ_1 and μ_k (known as extreme Ritz values) of the sequence tridiagonal matrix $\mathbf{T}_k = \mathbf{P}_k^{\mathrm{T}}\mathbf{AQ}_k$ (whose

eigenvalues are μ_i, $i = 1, \ldots, k$, with $|\mu_1| > \ldots \geq |\mu_k|$) derived from the biorthogonalisation of the left and right Krylov matrices $\mathbf{K}_k(\mathbf{A}, \mathbf{p}_1, k) = [\mathbf{p}_1, \mathbf{A}\mathbf{p}_1, \ldots, \mathbf{A}^{k-1}\mathbf{p}_1]$ and $\mathbf{K}_k(\mathbf{A}, \mathbf{q}_1, k) = [\mathbf{q}_1, \mathbf{A}\mathbf{q}_1, \ldots, \mathbf{A}^{k-1}\mathbf{q}_1]$, respectively, which span the *Krylov subspaces*,

$$\begin{aligned}\mathcal{K}_k(\mathbf{A}, \mathbf{p}_1, k) &= span\left\{\mathbf{p}_1, \mathbf{A}\mathbf{p}_1, \ldots, \mathbf{A}^{k-1}\mathbf{p}_1\right\}\\ \mathcal{K}_k(\mathbf{A}, \mathbf{q}_1, k) &= span\left\{\mathbf{q}_1, \mathbf{A}\mathbf{q}_1, \ldots, \mathbf{A}^{k-1}\mathbf{q}_1\right\},\end{aligned} \tag{6}$$

are gradually better estimates of λ_1 and λ_n.

The approximate left and right eigenvectors of $\mathbf{A}$ (known as Ritz vectors) are the columns of the matrices $\mathbf{W}_k = \mathbf{P}_k \left(\mathbf{V}_{T_k}^{-1}\right)^{\mathrm{T}} = [\mathbf{w}_1, \ldots, \mathbf{w}_k]$ and $\mathbf{V}_k = \mathbf{Q}_k\mathbf{V}_{T_k} = [\mathbf{v}_1, \ldots, \mathbf{v}_k]$, respectively, where $\mathbf{V}_{T_k}$ (whose columns must not be confused with the right Ritz vectors) is the matrix of the right eigenvectors of $\mathbf{T}_k$ (i.e., $\mathbf{T}_k\mathbf{V}_{T_k} = \mathbf{V}_{T_k}\mathbf{\Lambda}_{T_k}$).

B. Algorithm of the Non-Hermitian Lanczos Method

The non-Hermitian Lanczos method builds Krylov subspaces using biorthogonal Lanczos vectors to construct a tridiagonal matrix from the original matrix $\mathbf{A}$. The eigenvalues of the tridiagonal matrix are used to approximate the eigenvalues and both eigenvectors of $\mathbf{A}$ by the Rayleigh-Ritz procedure. That is, the method builds two biorthogonal matrices $\mathbf{P}_k = [\mathbf{p}_1, \ldots, \mathbf{p}_k]$ and $\mathbf{Q}_k = [\mathbf{q}_1, \ldots, \mathbf{q}_k]$ of Lanczos vectors ($\mathbf{P}_k^{\mathrm{T}}\mathbf{Q}_k = \mathbf{I}_k$) that progressively approximate the eigenvalues of $\mathbf{A}$ by the eigenvalues of the tridiagonal matrix $\mathbf{T}_k = \mathbf{P}_k^{\mathrm{T}}\mathbf{A}\mathbf{Q}_k$, i.e., by the Ritz values μ_i ($i = 1, \ldots, k$) [12], [13]. Thus, at any iteration k, it is verified that [13]

$$\begin{aligned}\mathbf{A}\mathbf{Q}_k &= \mathbf{Q}_k\mathbf{T}_k + \mathbf{r}_k\mathbf{e}_k^{\mathrm{T}}\\ \mathbf{A}^{\mathrm{T}}\mathbf{P}_k &= \mathbf{P}_k\mathbf{T}_k^{\mathrm{T}} + \mathbf{s}_k\mathbf{e}_k^{\mathrm{T}},\end{aligned} \tag{7}$$

where $\mathbf{e}_k$ is the k-th canonical basis vector of size k, and $\mathbf{r}_k$ and $\mathbf{s}_k$ are the Lanczos residual vectors, which can be expressed as [12], [13], [17], [18], [19], [20], [21], [22], [23]

$$\begin{aligned}||\mathbf{r}_k||_2 &= ||\mathbf{A}\mathbf{v}_i - \lambda_{T_i}\mathbf{v}_i||_2 \cdot |(\mathbf{V}_{T_k})_{ki}|^{-1}\\ ||\mathbf{s}_k||_2 &= \left|\left|\mathbf{A}^{\mathrm{T}}\mathbf{w}_i - \lambda_{T_i}\mathbf{w}_i\right|\right|_2 \cdot \left|\left(\mathbf{V}_{T_k}^{-1}\right)_{ki}^{\mathrm{T}}\right|^{-1},\end{aligned} \tag{8}$$

where $i = 1, \ldots, k$. The norms of the Lanczos residual vectors make it possible to estimate the proximity of the Ritz values and vectors to the eigenvalues and eigenvectors of the original matrix $\mathbf{A}$. They detect when the subspaces become invariant as a result of the Ritz subspaces becoming invariant; this is the case when $\mathbf{r}_k = 0$ or $\mathbf{s}_k = 0$.

In exact arithmetic, the non-Hermitian Lanczos method allows the tridiagonal matrix $\mathbf{T}_k$ to be computed with a fast convergence rate applying the following well-known algorithm for $k = 1$ to m (with $m < n$), which starts from arbitrary initial vectors $\mathbf{p}_1$ and $\mathbf{q}_1$ [13]:

$$\begin{aligned}\mathbf{T}_k = \mathbf{P}_k^{\mathrm{T}}\mathbf{A}\mathbf{Q}_k &= \begin{bmatrix}\alpha_1 & \gamma_1 & 0 & \ldots & 0\\ \beta_1 & \alpha_2 & \ddots & & \vdots\\ 0 & \ddots & \ddots & \ddots & 0\\ \vdots & & \ddots & \ddots & \gamma_{k-1}\\ 0 & \ldots & 0 & \beta_{k-1} & \alpha_k\end{bmatrix}\\ \alpha_k &= \mathbf{p}_k^{\mathrm{T}}\mathbf{A}\mathbf{q}_k,\ \mathbf{p}_1^{\mathrm{T}}\mathbf{q}_1 \neq 0\\ \mathbf{r}_k &= (\mathbf{A} - \alpha_k\mathbf{I})\,\mathbf{q}_k - \gamma_{k-1}\mathbf{q}_{k-1},\ \gamma_0\mathbf{q}_0 = 0\\ \mathbf{s}_k &= (\mathbf{A} - \alpha_k\mathbf{I})^{\mathrm{T}}\mathbf{p}_k - \beta_{k-1}\mathbf{p}_{k-1},\ \beta_0\,\mathbf{p}_0 = 0\\ \mathbf{q}_{k+1} &= \mathbf{r}_k \,/\, \beta_k \quad (\beta_k = ||\mathbf{r}_k||_2)\\ \mathbf{p}_{k+1} &= \mathbf{s}_k \,/\, \gamma_k \quad \left(\gamma_k = \mathbf{s}_k^{\mathrm{T}}\mathbf{r}_k \,/\, \beta_k\right).\end{aligned} \tag{9}$$

Unfortunately, the non-Hermitian Lanczos method can suffer from the loss of biorthogonality of the Lanczos vectors due to finite-precision calculations (roundoff error), which can lead to inaccurate Ritz values and vectors. This can be avoided using an alternative approach of the non-Hermitian Lanczos method called the non-Hermitian Lanczos method with full re-biorthogonalisation [12], [13]. This approach orthogonalises each newly computed Lanczos vector against all of its predecessors instead of just against the previous vector, helping to maintain biorthogonality and reducing accumulation errors. The method calculates the Krylov subspace vectors $\mathbf{A}^{k-1}\mathbf{q}_1$ and $\mathbf{A}^{k-1}\mathbf{p}_1$ at any iteration k, and the Gram-Schmidt orthogonalisation process is subsequently applied to these vectors to make them orthogonal to the previous Lanczos vectors (i.e., $\mathbf{q}_k$ w.r.t. $\mathbf{q}_{k-1}$ and $\mathbf{p}_k$ w.r.t. $\mathbf{p}_{k-1}$):

$$\begin{aligned}&\alpha_k = \mathbf{p}_k^{\mathrm{T}}\mathbf{A}\mathbf{q}_k,\ \mathbf{r}_k = \mathbf{A}\mathbf{q}_k,\ \ \mathbf{s}_k = \mathbf{A}^{\mathrm{T}}\mathbf{p}_k,\ \mathbf{p}_1^{\mathrm{T}}\mathbf{q}_1 \neq 0\\ &\mathbf{r}_k = \mathbf{r}_k - \sum_{i=1}^{k-1}\frac{\mathbf{q}_i\left(\mathbf{p}_i^{\mathrm{T}}\mathbf{r}_k\right)}{\mathbf{p}_i^{\mathrm{T}}\mathbf{q}_i} = \mathbf{r}_k - \sum_{i=1}^{k-1}\mathbf{q}_i\left(\mathbf{p}_i^{\mathrm{T}}\mathbf{r}_k\right)\\ &\mathbf{s}_k = \mathbf{s}_k - \sum_{i=1}^{k-1}\frac{\mathbf{p}_i\left(\mathbf{q}_i^{\mathrm{T}}\mathbf{s}_k\right)}{\mathbf{q}_i^{\mathrm{T}}\mathbf{p}_i} = \mathbf{s}_k - \sum_{i=1}^{k-1}\mathbf{p}_i\left(\mathbf{q}_i^{\mathrm{T}}\mathbf{s}_k\right)\\ &\mathbf{q}_{k+1} = \mathbf{r}_k \,/\, \beta_k \quad (\beta_k = ||\mathbf{r}_k||_2)\\ &\mathbf{p}_{k+1} = \mathbf{s}_k \,/\, \gamma_k \quad \left(\gamma_k = \mathbf{s}_k^{\mathrm{T}}\mathbf{r}_k \,/\, \beta_k\right).\end{aligned} \tag{10}$$

It is often recommended to apply the Gram-Schmidt process *twice* to ensure the biorthogonality of the Krylov subspace vectors [12], [13]. It must be noted that the algorithm (10) will be applied at each frequency (i.e., $\mathbf{A} = \mathbf{Y}_{\mathbf{B},f}$) over the frequency range studied by RMA (see Section IV).

According to (8), an algorithm termination (or stopping criterion) based on the subspaces invariance could be defined by using the norms of the Lanczos residual vectors [12], [13], [17], [18], [19], [20], [21], [22], [23]. However, the entire subspaces invariance can be an extremely demanding criterion. For this reason, as the objective is to find the extreme modulus eigenvalues of $\mathbf{A}$, a stopping criterion based on them, such as (4) [15],

TABLE I
NON-HERMITIAN LANCZOS ALGORITHM WITH FULL RE-BIORTHOGONALISATION

1:	$\mathbf{Q}_1 = \mathbf{q}_1 = \frac{\mathbf{v}}{\|\mathbf{v}\|_2}$, $\mathbf{P}_1 = \mathbf{p}_1 = \frac{\mathbf{w}}{\|\mathbf{w}\|_2}$, $\mathbf{p}_1^{\mathrm{T}}\mathbf{q}_1 \neq 0$
2:	***for*** $k = 1 : m_{mx}$
3:	$\alpha_k = \mathbf{p}_k^{\mathrm{T}}\mathbf{A}\mathbf{q}_k$, $\mathbf{r}_k = \mathbf{A}\mathbf{q}_k$, $\mathbf{s}_k = \mathbf{A}^{\mathrm{T}}\mathbf{p}_k$
4:	$\mathbf{r}_k = \mathbf{r}_k - \sum_{i=1}^{k} \mathbf{q}_i(\mathbf{p}_i^{\mathrm{T}}\mathbf{r}_k) = \mathbf{r}_k - \mathbf{Q}_k(\mathbf{P}_k^{\mathrm{T}}\mathbf{r}_k)$ *(twice)*
5:	$\mathbf{s}_k = \mathbf{s}_k - \sum_{i=1}^{k} \mathbf{p}_i(\mathbf{q}_i^{\mathrm{T}}\mathbf{s}_k) = \mathbf{s}_k - \mathbf{P}_k(\mathbf{Q}_k^{\mathrm{T}}\mathbf{s}_k)$ *(twice)*
6:	*calculate/update* $\mathbf{T}_k$ *with* α_k, β_{k-1} *and* γ_{k-1}
7:	*compute the Ritz values, i.e., the eigenvalues* $\mathbf{\Lambda}_{T_k}$
8:	***if*** $\epsilon^{(k)} = \left\|\sigma^{(k)} - \sigma^{(k-1)}\right\| / \left\|\sigma^{(k-1)}\right\| < \Sigma$ $\rightarrow$ ***break***
9:	$\beta_k = \|\mathbf{r}_k\|_2$, $\gamma_k = \mathbf{s}_k^{\mathrm{T}}\mathbf{r}_k / \beta_k$
10:	$\mathbf{q}_{k+1} = \mathbf{r}_k / \beta_k$, $\mathbf{p}_{k+1} = \mathbf{s}_k / \gamma_k$
11:	$\mathbf{Q}_{k+1} = [\mathbf{Q}_k, \mathbf{q}_{k+1}]$, $\mathbf{P}_{k+1} = [\mathbf{P}_k, \mathbf{p}_{k+1}]$
12:	***end for***
13:	*compute the right eigenvectors* $\mathbf{V}_{T_k}$ *of* $\mathbf{T}_k$
14:	*compute the Ritz vectors* $\mathbf{V}_k = \mathbf{Q}_k\mathbf{V}_{T_k}$ *and* $\mathbf{W}_k = \mathbf{P}_k(\mathbf{V}_{T_k}^{-1})^{\mathrm{T}}$

is finally applied, i.e.,

$$\epsilon^{(k)} = \frac{\left|\sigma^{(k)} - \sigma^{(k-1)}\right|}{\left|\sigma^{(k-1)}\right|} < \Sigma, \tag{11}$$

where Σ (e.g., $\Sigma = 10^{-10}$) is the tolerance set to define when the algorithm stops, and σ are the Ritz values calculated at each iteration. Additionally, a maximum number of Lanczos iterations m_{mx} (where always $m_{mx} < n$) is selected for the construction and sizing of the Krylov subspace to avoid unnecessary iterations in case of convergence problems of the Lanczos method.

Table I summarises the non-Hermitian Lanczos algorithm with full re-biorthogonalisation. Two final recommendations are given to improve computational efficiency of the algorithm in Table I. First, the use of restart techniques [13], [21], [22], particularly when dealing with large-scale eigenvalue problems. This allows better memory management and adaptability to specific eigenvalue clusters. Second, the use of the shift-and-invert transformation, which consists of defining the eigenproblem as $(\mathbf{A} - d{\cdot}\mathbf{I})^{-1}\mathbf{x} = \rho\mathbf{x}$, where $\rho = 1 \,/\, (\lambda - d)$. This transformation can significantly improve the convergence rate, making the algorithm more efficient for computing eigenvalues with specific properties, such as the smallest modulus eigenvalues.

C. Suitability of the Non-Hermitian Lanczos Method

This Subsection aims to answer the following question: *Why is it better to use the non-Hermitian Lanczos method instead of other methods?* Several methods exist in the literature for solving eigenproblems (e.g., the QR method, Jacobi method, PI method, Lanczos method, and Arnoldi method) [12], [13], [17], [18], [19], [20], [21], [22], [23], [24], [25], [26]. The most suitable ones for RMA studies of large transmission grids are the PI, non-Hermitian Lanczos, and Arnoldi methods.

The convergence of the PI method is geometric [13], i.e., the modulus of the difference between the true and the computed extreme modulus eigenvalues decreases geometrically at each iteration with the ratio of the second to the first extreme modulus eigenvalues (see Section II-B). Let $C^{(k)}$ be the upper bound for the modulus of the above difference. Regarding the Lanczos method, let $D^{(k)}$ be the upper bound for the modulus of the same difference. It is verified that $D^{(k)} < C^{(k)}$ [13], i.e., at each iteration k, the estimates of the extreme modulus eigenvalues obtained by the Lanczos method are better than those obtained by the PI method, leading to faster convergence. This is because the Lanczos method computes the associated extreme modulus eigenpairs at each iteration k considering all previously calculated vectors (see Section III-B), whereas the PI method considers only the previously calculated vector (see Section II-B).

Moreover, the non-Hermitian Lanczos method is an iterative algorithm that computes a few selected eigenvalues and eigenvectors of a large sparse matrix. It does not exploit matrix sparsity directly but the inherent characteristics of sparse matrices, such as more efficient matrix-vector multiplications, reduced memory requirements and selective computation, making the Lanczos method a practical and effective approach for eigenvalue computation in sparse settings. The leverage of matrix sparsity by this method can be summarised in the following three aspects [26]:

- *Efficient matrix-vector multiplications:* It is widely known that matrix-vector multiplications involving sparse matrices can be performed more efficiently than those involving dense matrices. This is crucial in the Lanczos method because it repeatedly multiplies the matrix with a vector during the iteration process. Sparsity allows faster computation and reduces memory requirements.
- *Reduction of storage requirements:* Since the tridiagonal matrix (9) generated by the Lanczos method is much smaller than the original matrix, storage requirements are significantly reduced. This is especially beneficial when dealing with large sparse matrices, as the algorithm can handle matrices that might be infeasible to store explicitly.
- *Selective computation of eigenvalues:* The selective computation of eigenvalues performed by the Lanczos method requires less overall computational cost than the computation of all eigenvalues. The sparsity of the matrix can help identify the desired eigenvalues more efficiently since the Lanczos process tends to focus on the dominant components of the matrix, which are often associated with non-zero entries.

The Arnoldi method is the most popular *Krylov subspace* method for solving non-Hermitian eigenproblems of large, sparse matrices [18], [22]. However, comparative studies between the Arnoldi method and the non-Hermitian Lanczos method do not favour either method, and the choice between the two methods is at the discretion of the user [20], who is guided by their advantages and disadvantages, as well as the characteristics

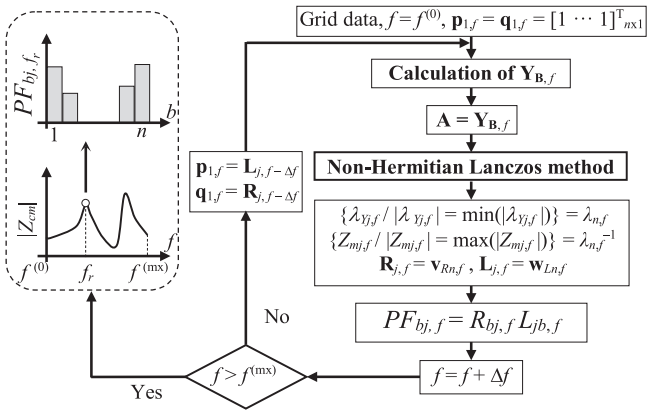

Fig. 3. Flowchart of L_RMA.

of the studied matrix. The non-Hermitian Lanczos method offers several advantages over the Arnoldi method that enhance RMA studies [18], [21]:

- High accuracy: Concerning the approximation of eigenvalues, it can be stated from [18] that the non-Hermitian Lanczos method is more accurate than the Arnoldi method.
- Lower computational memory requirements: A comparison in [21] between different algorithms for non-Hermitian matrix eigenproblems concludes that the non-Hermitian Lanczos method requires less computational memory than other methods (including the Arnoldi method) for the same workload.
- Ability to obtain both the left and right eigenvectors at the end of the iteration process: This is a significant advantage for RMA studies.

IV. Lanczos Method-Based Resonance Mode Analysis

The usefulness of r_RMA is compromised when large multi-terminal transmission grids with a high number of eigenvalues must be studied [11]. In this case, the non-Hermitian Lanczos method is a powerful tool to use in RMA to investigate this type of grids characterised by large non-Hermitian admittance matrices $\mathbf{Y}_{\mathbf{B},f}$. Moreover, as the grid grows, these matrices become sparse (i.e., most of their coefficients are zero), enabling the use of sparse matrix techniques [29], [30]. Therefore, for large multi-terminal transmission grids with sparse admittance matrices, L_RMA, which applies the non-Hermitian Lanczos method with full re-biorthogonalisation in the RMA (see Section III-B), is strongly recommended.

Fig. 3 shows the L_RMA flowchart. L_RMA involves setting $\mathbf{A}=\mathbf{Y}_{\mathbf{B},f}$ at every frequency f over the frequency range, and the non-Hermitian Lanczos method with full re-biorthogonalisation (see Table I) can find an approximation at each frequency of the smallest modulus eigenvalue $\lambda_{Yj,f}=\lambda_{n,f}$ of $\mathbf{Y}_{\mathbf{B},f}$ and the corresponding left and right unit eigenvectors $\mathbf{L}_{j,f}$ and $\mathbf{R}_{j,f}$, respectively. Based on this eigen-triplet $(\mathbf{L}_{j,f},\lambda_{Yj,f},\mathbf{R}_{j,f})$, the resonance modal impedance of $\mathbf{Z}_{\mathbf{B},f}$ is computed as $Z_{mj,f}=1/\lambda_{Yj,f}$, and the associated left and right unit eigenvectors coincide with $\mathbf{L}_{j,f}$ and $\mathbf{R}_{j,f}$. Hence, L_RMA allows the evolution envelope of the moduli of all modal impedances $Z_{mj,f}$ of $\mathbf{Z}_{\mathbf{B},f}$ over the entire frequency range to be calculated, known as $|Z_{cm}|$ (5).

In order to apply the non-Hermitian Lanczos method in L_RMA, the following must be considered:

- In L_RMA, the non-Hermitian Lanczos method algorithm computes eigenpairs of $\mathbf{T}_k$ at every frequency over the frequency range, which converge to the Ritz values and vectors approximations $(\mathbf{w}_{i,f},\mu_{i,f},\mathbf{v}_{i,f})$, $i=1,\ \ldots,\ k$. Thus, RMA requires only the smallest modulus eigenvalue $\lambda_{n,f}$ and its eigenvectors $\mathbf{w}_{Ln,f}$ and $\mathbf{v}_{Rn,f}$ of $\mathbf{Y}_{\mathbf{B},f}$,
$$\lambda_{n,f}=\mu_{k,f},\ \mathbf{w}_{Ln,f}=\mathbf{w}_{k,f},\ \mathbf{v}_{Rn,f}=\mathbf{v}_{k,f}, \tag{12}$$
where $(\mathbf{w}_{k,f},\mu_{k,f},\mathbf{v}_{k,f})$ is the eigen-triplet associated with the Ritz value of smallest modulus. Consequently, the left and right unit eigenvectors will be $\mathbf{L}_{j,f}=\mathbf{w}_{Ln,f}$ and $\mathbf{R}_{j,f}=\mathbf{v}_{Rn,f}$, respectively.
- The $\mathbf{p}$ and $\mathbf{q}$ vectors of the Lanczos algorithm must always satisfy the orthogonality condition, i.e., $\mathbf{p}_k^{\mathrm{T}}\,\mathbf{q}_k=0$. This need not be the case for the algorithm's initialisation vectors, i.e., $\mathbf{p}_1^{\mathrm{T}}\mathbf{q}_1\neq 0$. As with the initialisation for the PI-based method in Section II-B, the left and right eigenvectors at the previous frequency are good starting vectors $\mathbf{p}_1$ and $\mathbf{q}_1$, respectively, while the starting vectors at the first frequency are chosen as $\mathbf{p}_1=\mathbf{q}_1=[1\ \cdots\ 1]^{\mathrm{T}}_{n\times 1}$ [13], [23], i.e.,
$$\mathbf{p}_{1\,f^{(0)}}=\mathbf{q}_{1\,f^{(0)}}=\frac{\mathbf{z}_1}{||\mathbf{z}_1||_2},\ \mathbf{z}_1=[1\ \cdots\ 1]_{n\times 1},$$
$$\mathbf{p}_{1\,f\neq f^{(0)}}=\mathbf{L}_{j,\,f-\Delta f},\ \mathbf{q}_{1\,f\neq f^{(0)}}=\mathbf{R}_{j,\,f-\Delta f}. \tag{13}$$
- The use of the shift-inverted transformation means that matrix $\mathbf{A}$ in Table I must be defined as follows: $\mathbf{A}=(\mathbf{Y}_{\mathbf{B},f}-d\cdot\mathbf{I})^{-1}$. Consequently, the eigenvalue of $\mathbf{A}$ in this case is $\lambda_{n,f}=1\ /\ \mu_{k,f}+d$, while the eigenvectors remain unchanged; that is, they are the same as the eigenvectors of $\mathbf{Y}_{\mathbf{B},f}$. Setting d as the eigenvalue obtained at the previous frequency is a good approximation, while $d=0$ for the first frequency, i.e.,
$$d_{f^{(0)}}=0,\quad d_{f\neq f^{(0)}}=\lambda_{n,\,f-\Delta f}. \tag{14}$$

In Section VI, it is numerically verified that L_RMA requires less computational time than r_RMA for large, sparse admittance matrix scenarios without loss of accuracy.

A numerical example of the non-Hermitian Lanczos algorithm with full re-biorthogonalisation (see Table I) application to the admittance matrix of IEEE 3-bus test power system at 100 Hz is described step by step at the end of the paper (see Appendix section).

V. Resonance Mode Analysis-Based Methodology

An RMA-based methodology that incorporates both r_RMA and L_RMA approaches is proposed. It should be noted that these approaches can be applied to assess resonances and stability issues across any poorly damped frequency range, as such scenarios typically result in singularities in the admittance matrix $\mathbf{Y}_{\mathbf{B},f}$ and peak values of the $\mathbf{Z}_{\mathbf{B},f}$ components (1) at resonance frequencies [7]. Moreover, since the above approaches

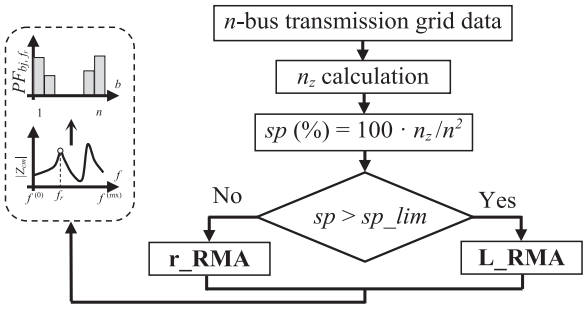

Fig. 4. Flowchart of RMA-based methodology.

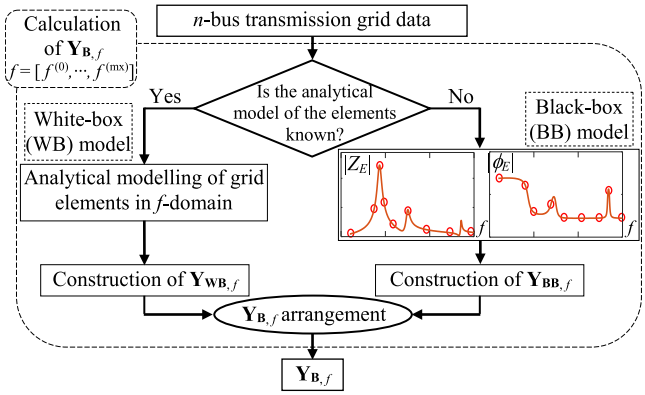

Fig. 5. Flowchart of the admittance matrix calculation.

are based on the construction of the admittance matrix, they can be applied regardless of the VSC model and are suitable for both synchronous and harmonic frequency ranges. The integration of black-box models for transmission grid components without analytical models in the methodology is also described.

A. Description of the Methodology

The flowchart of an RMA-based methodology for studying resonances in transmission grids is presented in Fig. 4, incorporating both r_RMA (see basics in Section II-B and flowchart in Fig. 2) and L_RMA (see basics in Section IV and flowchart in Fig. 3) approaches. It should be noted that the proposed RMA-based methodology combines these two approaches appropriately based on the results obtained in Section VI, where it is numerically verified that L_RMA requires less computational time than r_RMA for large, sparse admittance matrix scenarios, while r_RMA remains the most efficient approach for small transmission grids.

Thus, two different paths (r_RMA or L_RMA) based on the sparsity ratio of the nxn grid admittance matrix $\mathbf{Y_B}$ are proposed for RMA studies [27],

$$sp(\%) = 100\frac{n_z}{n^2}, \tag{15}$$

where $n_z = n^2 - n - 2n_r$ is the total number of zero elements within $\mathbf{Y_B}$, and n_r is the number of branches in the grid that connect two buses other than the reference bus. If $sp > sp\_lim$, then the sparsity of $\mathbf{Y_B}$ recommends using L_RMA; otherwise, r_RMA is the better choice. The numerical study in Section VI concludes that setting *sp_lim* to 98% is reasonable.

Sparsity ratio, *sp*, is highly related to grid size. Large transmission grids with approximately more than 200 buses typically have an admittance matrix with sparsity as high as 97% because of the limited connections between buses and the large number of zero elements in the admittance matrix [28].

It should be noted that, according to the study performed in Section VI-A2), f_RMA might be a better option than r_RMA in the flowchart of the RMA-based methodology (see Fig. 4), with the same scope of applicability as that of r_RMA compared to that of L_RMA for resonance studies in transmission grids.

For enhanced reader understanding of the specific application process of the RMA-based methodology regarding the path of the L_RMA approach in the flowchart in Fig. 4, it is strongly recommended to analyse in detail the numerical example presented at the end of Section IV.

B. Integration of Black-Box Models

Often, the white-box models of specific transmission grid components, such as certain power electronics-based components and inverter-based resources, are unavailable. Instead, their impedance/admittance frequency profiles are typically provided by manufacturers or obtained through measurements in the form of black-box models. In such scenarios, these black-box models can be integrated into the calculation of the admittance matrix $\mathbf{Y_{B},}_f$ at each frequency (1). Subsequently, the RMA-based methodology can be applied to this admittance matrix to investigate resonances.

The flowchart in Fig. 5 outlines the procedure for computing the admittance matrix using both white-box and black-box models of the transmission grid components, thereby bridging the gap between these two modelling approaches in resonance analyses. It is important to note that discretising the black-box models into smaller frequency intervals is essential to avoid overlooking critical regions of the impedance/admittance frequency plots, as this could result in inaccurate characterisation of resonance frequencies.

VI. Application

This Section analyses and compares the four RMA-based approaches presented in the paper (RMA, r_RMA, f_RMA, and L_RMA) using ten IEEE test power systems (IEEE 3– [31], 5– [32], 9– [33], 14– [34], 24– [35], 30– [36], 39– [37], 57– [38], 118– [39], and 300– [40] bus) and seven synthetic test power systems (Central Illinois 200– [41], South Carolina 500– [42], Texas 2k– [43], Texas 7k– [44], East Coast USA 10k– [45], North Central USA 25k – [45] and Eastern USA 70k– [45] bus). First, the accuracies of r_RMA, f_RMA, and L_RMA are validated by MATSIM frequency scans of the IEEE 5– and 14– bus test power systems. After validation, the convergence times of the four RMA-based approaches are compared for all the test power systems and their accuracies are checked with the 39–, 57– and 118– bus test power systems. Second, the

application of the PFs obtained by L_RMA is illustrated by MATSIM numerical simulations of the IEEE 5−bus test power system. Finally, a small-signal stability study of the modified IEEE 118−bus test power system is performed by L_RMA. The RMA algorithms apply a fixed frequency step of 1 Hz during the simulations. A variable frequency step could be used to avoid calculations associated with eigenvalue conflict frequencies and focus only on obtaining accurate resonance frequencies [15]. However, the choice of a smart variable frequency step is not trivial and resonance frequencies might be skipped in large multi-terminal transmission grids with multiple close resonance frequencies. The applied tolerances for the numerical methods used (i.e., PI method or non-Hermitian Lanczos method) are $\Delta = 10^{-10}$, $\delta = 10^{-6}$ and $\Sigma = 10^{-10}$, as previously proposed in Sections II-B (see (4)) and III-B (see (11)). It is recommended (as done in this study) to use sparsity techniques [29], [30], especially in scenarios involving large admittance/impedance matrices.

A. Accuracies and Convergence Times of the RMA-Based Approaches

The accuracies and convergence times of the RMA-based approaches are analysed in two different studies:

1) Comparison of the RMA-Based Approaches vs. MATSIM: The IEEE 5− [32] and 14− [34] bus test power systems are used to validate the accuracies of r_RMA, f_RMA, and L_RMA by MATSIM simulation (see Fig. 6). It is observed that r_RMA, f_RMA, and L_RMA assess the resonance phenomenon easily because they summarise the frequency behaviour of the grid using the critical mode impedance, thus avoiding the need to study all the grid impedances. The resonance frequencies of $|Z_{cm}|$ obtained by r_RMA, f_RMA, and L_RMA are compared with the resonance frequencies of the driving point impedances $|Z_{bb}|$ obtained by MATSIM simulation.

Accuracy is thoroughly investigated by comparing the r_RMA, f_RMA, and L_RMA resonance frequencies with the MATSIM resonance frequencies using the percentage of error $\zeta_{f_r,i}$, i.e.,

$$\zeta_{f_r,i} = 100\frac{|\,f_{r,\mathrm{MATSIM}} - f_{r,i}|}{f_{r,\mathrm{MATSIM}}}, i = a\_\mathrm{RMA}\ (a = \mathrm{r},\ \mathrm{f},\ \mathrm{L}). \tag{16}$$

This error is assessed by studying the resonance frequencies with a 0.001 Hz frequency step. The percentage of error $\zeta_{f_r,i}$ is below 0.01% (as labelled in Fig. 6), thus validating that the r_RMA, f_RMA, and L_RMA results reveal the resonance frequencies of the driving point impedances accurately.

2) Comparison Between the RMA-Based Approaches: RMA, r_RMA, f_RMA, and L_RMA convergence times with increased grid size and the sparsity ratio *sp* of the grid admittance matrices are shown in Fig. 7. To calculate them, the average time of a number of simulations of the ten IEEE and seven synthetic test power systems over the 100 to 3000 Hz frequency range (1 Hz step size) was determined. It is worth noting that the times displayed only correspond to the duration required to apply the specific RMA-based approach. Therefore, the construction of

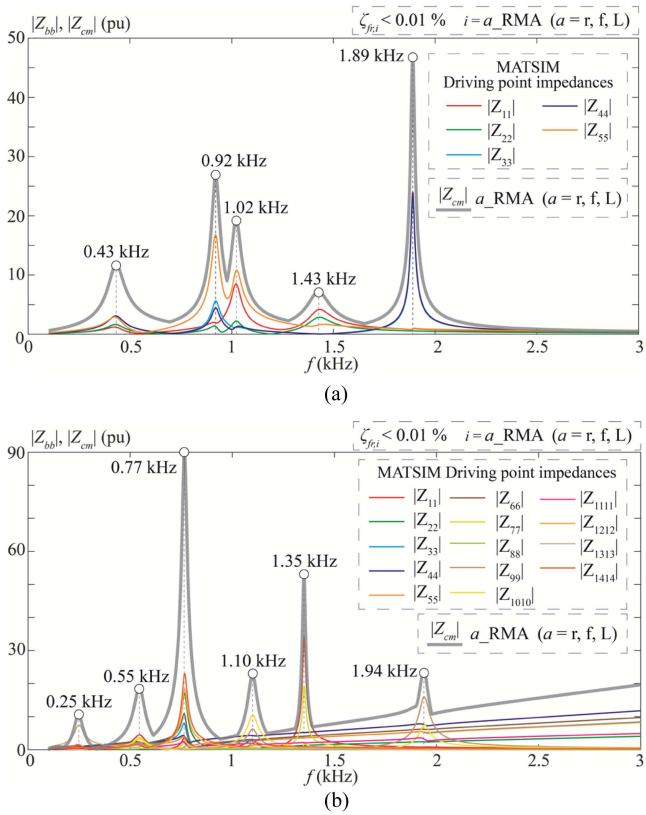

Fig. 6. Resonance assessment of the IEEE 5– (a) and IEEE 14– (b) bus test power systems by MATSIM frequency scan, r_RMA, f_RMA, and L_RMA.

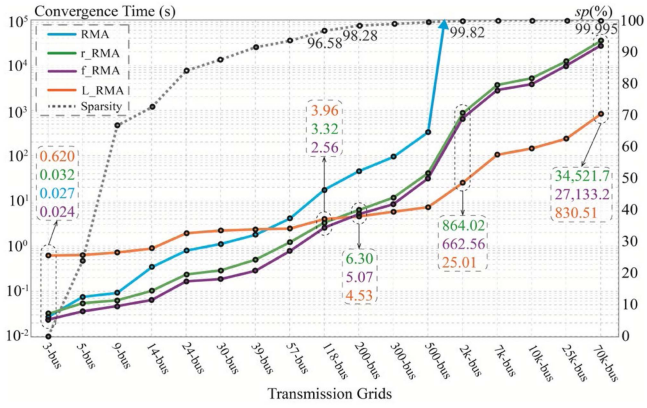

Fig. 7. Convergence times and *sp* as a function of the test power systems.

the grid admittance matrix is not considered at this stage. These simulations were made using MATLAB/Simulink R2022b version on a Windows 11 Pro 64-bit system featuring a 13th Gen Intel Core$^{\mathrm{TM}}$ i9-13900K CPU with a clock speed of 3.00 GHz, 32 cores and x64 architecture. The system was also equipped with 64 GB DDR5 5600MHz RAM, two SSD storage units WD BLACK SN850X 2TB NVME M.2 2280, and a NVIDIA GeForce RTX 4090 24GB VERTO GPU.

The results in Fig. 7 indicate that r_RMA and f_RMA are the best approaches for *sp* values below 98%, while L_RMA is more efficient than RMA and r_RMA when *sp* rises above 98%. Note

that f_RMA always outperforms r_RMA, as extensively analysed in [16]. The high efficiency of L_RMA in studies with large, sparse admittance matrices is especially confirmed in the cases between the 2k−bus and 70k−bus grids. For example, L_RMA is 97% and 96% faster than r_RMA and f_RMA, respectively, for the Texas 2k−bus test power system with $sp = 99.82\%$. Furthermore, when analysing the East USA 70k−bus test case with $sp = 99.995\%$, a significant difference can be observed (i.e., nearly 10 hours and 7.5 hours of computational time for r_RMA and f_RMA, respectively, versus only 14 minutes for L_RMA). It must be noted that the narrow distribution of critical eigenvalues in large transmission grids also contributes to the inefficiency of r_RMA compared to L_RMA. In such cases, f_RMA is a novel alternative to overcome r_RMA inefficiency, but it is also far less efficient than L_RMA. As discussed in Section III-C, L_RMA offers better and faster convergence than r_RMA and f_RMA. Considering the above RMA-based approaches, a methodology to assess resonances in transmission grids is proposed in Section V.

Fig. 8 compares the RMA, r_RMA, f_RMA, and L_RMA accuracy results for the IEEE 39−, 57− and 118− bus test power systems (only the resonance frequencies of the critical mode impedance with the largest modulus are labelled). It is observed that the results are identical. In order to check the accuracy numerically, the moduli of the critical resonance modes at f_r (i.e., $|Z_{cm,f_r}|$, or equivalently, (5) at f_r) and the resonance frequencies f_r are analysed using the percentage of errors $\zeta_{Z_{cm,f_r,i}}$ and $\zeta_{f_r,i}$, i.e.,

$$\zeta_{Z_{cm,f_r,i}} = 100\frac{\left||Z_{cm,f_r}|_{\text{RMA}} - |Z_{cm,f_r}|_i\right|}{|Z_{cm,f_r}|_{\text{RMA}}}$$

$$\zeta_{f_r,i} = 100\frac{|f_{r,\text{RMA}} - f_{r,i}|}{f_{r,\text{RMA}}}, i = a\_\text{RMA}\ (a = \text{r},\ \text{f},\ \text{L}). \tag{17}$$

This error is assessed by studying the resonance frequencies with a 0.001 Hz frequency step. The percentage of errors $\zeta_{Z_{cm,f_r,i}}$ and $\zeta_{f_r,i}$ is below 0.01%, as labelled in Fig. 8. The same holds true for the remaining transmission grids.

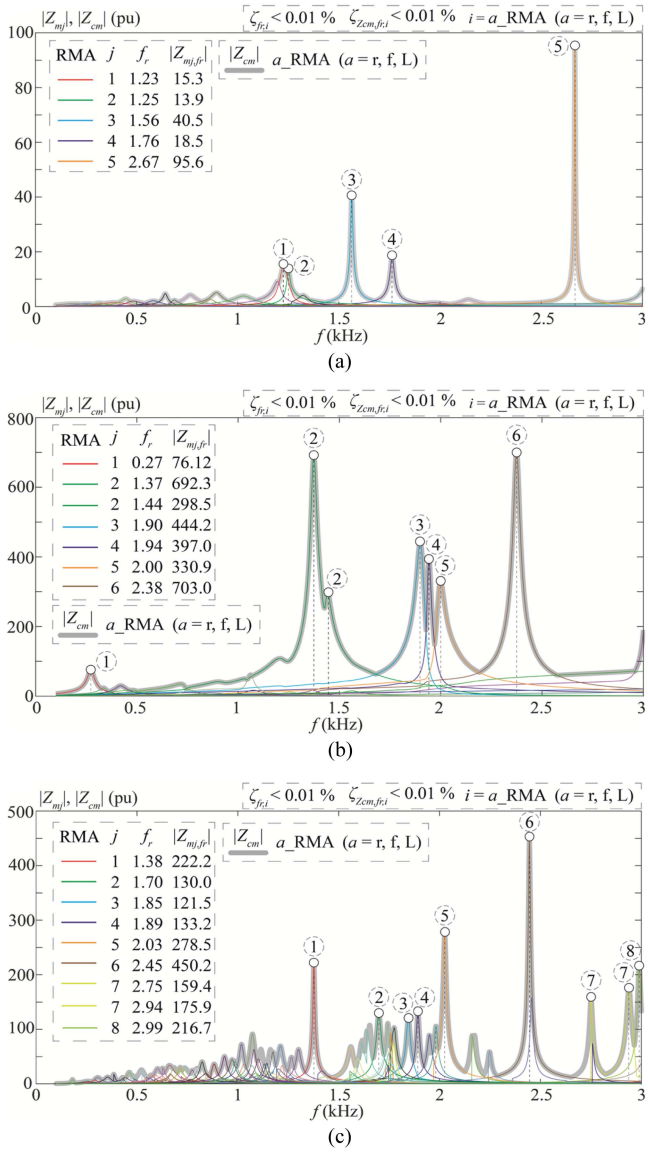

Fig. 8. Resonance characterisation of the IEEE 39– (a), IEEE 57– (b) and IEEE 118– (c) bus test power systems by RMA, r_RMA, f_RMA and L_RMA.

B. Application of the PFs

The four RMA-based approaches provide PFs that characterise the observability and excitability of the critical modes for each bus of the grid. This means that buses with higher PFs have a higher pollution level when harmonic currents are injected at the resonance frequency of the critical mode (observability), and the highest pollution level also occurs when harmonic currents are injected into these buses (excitability).

As an example, Fig. 9(a) shows the PFs of the five critical resonance modes of the IEEE 5−bus test power system (see Fig. 6) obtained by L_RMA. These PFs reveal that the second resonance frequency at 0.92 kHz is mostly influenced by bus 5, and the fifth resonance frequency at 1.89 kHz is only influenced by buses 3 and 4. The observability and excitability at the resonance frequency of 0.92 kHz are validated in Fig. 9(b) and (c) by MATSIM simulation. Fig. 9(b) shows the magnitude of the voltages at all buses of the transmission grid when a 0.05 pu harmonic current at 0.92 kHz is injected into each bus. Fig. 9(c) shows the time-domain waveforms of these voltages obtained by MATSIM simulation. The highest excitability of bus 5 at 0.92 kHz can be observed because the maximum voltage occurs when the current is injected into bus 5. Accordingly, the voltage values decrease progressively when a current is injected into the buses with lower PFs. Observability is demonstrated by the fact that bus 5 consistently exhibits the most pronounced (observed) voltage, regardless of the injection location. Moreover, the voltage values observed in the other buses are directly related to the magnitude of the PFs. It is also numerically verified that if harmonic currents are injected at frequencies other than the resonance frequencies, the resulting values of harmonic voltages are significantly lower than the values obtained in the example in Fig. 9 (i.e., the risk of overvoltage is much lower when injecting harmonic currents at non-resonance frequencies).

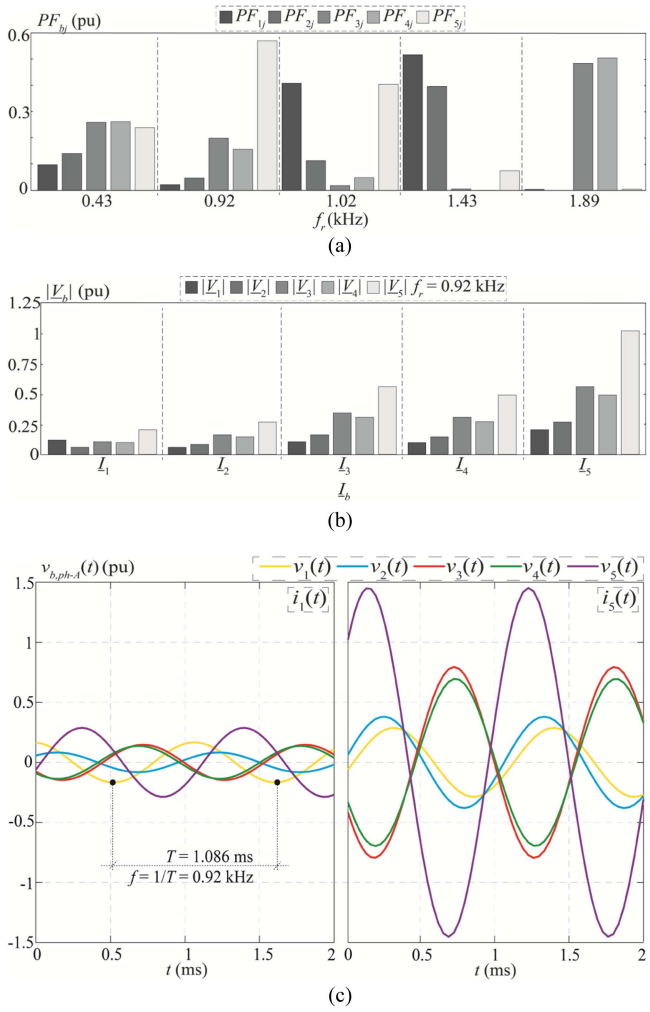

Fig. 9. Harmonic power quality study in the IEEE 5-bus test power system: (a) participation factors. (b) Influence of 0.92 kHz injected currents on voltages. (c) Time domain simulation of the influence of 0.92 kHz currents injected into bus 1 (left) and bus 5 (right) on voltages.

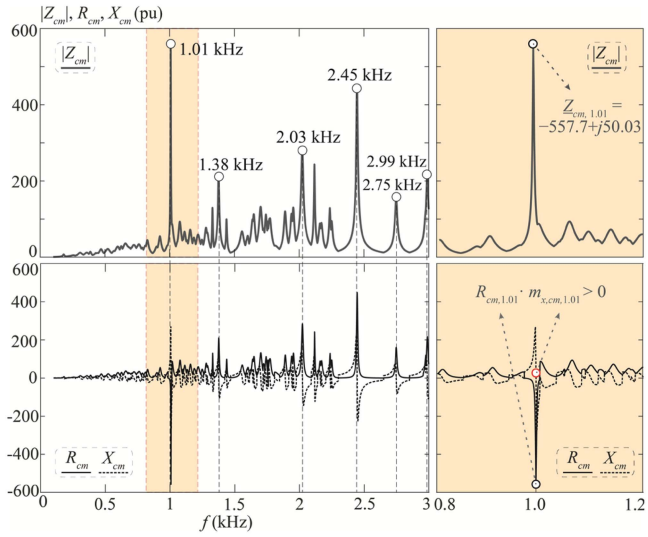

Fig. 10. Stability assessment of the modified IEEE 118-bus test power system using the PMD stability criterion by L_RMA.

C. Small-Signal Stability Study

In this Subsection, small-signal *converter-driven instabilities* [46] are analysed using the PMD stability criterion [7] to demonstrate the application of L_RMA in power system stability studies in large multi-terminal transmission grids. The PMD stability criterion states that the grid is stable iff (see details in [7])

$$m_{x_{cm},f_r} \cdot R_{cm,f_r} < 0$$
$$\left(m_{x_{cm},f_r} = \frac{\partial X_{cm,f_r}}{\partial f}\bigg|_{f=f_r},\ j = 1,\ \ldots, n\ \forall f_r \right) \quad (18)$$

where R_{cm,f_r} and X_{cm,f_r} are the real and imaginary parts of the critical resonance modes Z_{cm,f_r}, respectively, and m_{x_{cm},f_r} is the slope of X_{cm,f_r}.

The application of L_RMA using the PMD stability criterion is performed in the modified IEEE 118–bus test power system, where five identical VSCs with the parameters proposed in [7] are connected to buses 7, 23, 50, 79, and 101. In the scenario under study, the real and imaginary parts of the power system critical modes obtained by L_RMA in the frequency range from 0.1 to 3 kHz are analysed (see Fig. 10). These critical modes have multiple resonance frequencies, and the power system is predicted to be unstable. According to (18), this conclusion arises from observing that the product of the slope of $X_{mj,1.01}$ and the real component of the impedance mode $R_{mj,1.01}$ of the critical resonance mode at 1.01 kHz is greater than zero. The PFs of the unstable critical resonance mode at 1.01 kHz reveal that buses 7 and 117 have the most significant impact on this unstable critical resonance mode. Consequently, the VSC connected to bus 7 seems to be the primary contributor to the instability issue (PFs results are omitted for brevity).

Comparing Figs. 10 to 8(c) reveals that the frequency response remains largely consistent, although with noticeable influence from the presence of VSCs, particularly on the resonance patterns and their magnitudes. A clear example of this influence is the increased resonance at 1.01 kHz, coinciding with the point of instability.

Finally, the computational times for stability assessment are obtained using the four RMA approaches: RMA required 54.27 s, r_RMA 12.82 s, f_RMA 9.54 s, and L_RMA 8.13 s. Interestingly, unlike pure RMA computation, additional calculations to assess stability position L_RMA as the method with the most efficient time performance. However, r_RMA, f_RMA, and L_RMA times are quite similar, as also observed for the IEEE 118−bus test power system case in Fig. 7. This is because the sparsity of this grid is close to 98%, which is the limit of application for r_RMA, f_RMA, and L_RMA. Additionally, note that the times are slightly longer than those in Fig. 7 because a complete stability analysis is conducted instead of focusing only on resonances.

TABLE II
NON-HERMITIAN LANCZOS ALGORITHM WITH FULL RE-BIORTHOGONALISATION APPLICATION TO THE ADMITTANCE MATRIX OF THE IEEE 3-BUS TEST POWER SYSTEM AT 100 HZ

$$\mathbf{A} = \left(\mathbf{Y}_{\mathbf{B},\,100\,\mathrm{Hz}} - d\cdot\mathbf{I}\right)^{-1} = \left(\begin{bmatrix} 5.89 - j32.87 & -2.94 + j11.77 & -2.70 + j16.22 \\ -2.94 + j11.77 & 9.82 - j33.19 & -4.71 + j18.82 \\ -2.70 + j16.22 & -4.71 + j18.82 & 7.66 - j39.94 \end{bmatrix} - d\cdot\mathbf{I}\right)^{-1}, \quad d = 0,$$

where $\mathbf{\Lambda}_{\mathbf{Y_B},\,100\,\mathrm{Hz}} = [12.29 - j56.93 \quad 10.15 - j44.93 \quad 0.93 - j4.13]^{\mathrm{T}}$.

Algorithm		Numerical Example	
1:	$\mathbf{Q}_1 = \mathbf{q}_1 = \frac{\mathbf{v}}{\lVert\mathbf{v}\rVert_2}$, $\mathbf{P}_1 = \mathbf{p}_1 = \frac{\mathbf{w}}{\lVert\mathbf{w}\rVert_2}$, $\mathbf{p}_1^{\mathrm{T}}\mathbf{q}_1 \neq 0$	**Initialisation:** $\mathbf{v} = \mathbf{w} = [1\ 1\ 1]^{\mathrm{T}}$, $\mathbf{Q}_1 = \mathbf{P}_1 = [0.577\ 0.577\ 0.577]^{\mathrm{T}}$	
2:	***for*** $k = 1 : m_{mx}$	**Iteration 1**	**Iteration 2**
		$k = 1$	$k = 2$
3:	$\alpha_k = \mathbf{p}_k^{\mathrm{T}}\mathbf{A}\mathbf{q}_k$, $\mathbf{r}_k = \mathbf{A}\mathbf{q}_k$, $\mathbf{s}_k = \mathbf{A}^{\mathrm{T}}\mathbf{p}_k$	$\alpha_1 = 0.052 + j0.23$, $\mathbf{r}_1 = \mathbf{s}_1 = \begin{bmatrix} 0.027 + j0.13 \\ 0.035 + j0.14 \\ 0.028 + j0.13 \end{bmatrix}$	$\alpha_2 = 0.0053 + j0.020$, $\mathbf{r}_2 = \begin{bmatrix} 0.0045 - j0.0085 \\ 0.0006 + j0.019 \\ 0.0030 - j0.0023 \end{bmatrix}$, $\mathbf{s}_2 = \begin{bmatrix} -0.0029 - j0.0092 \\ 0.014 + j0.013 \\ 0.0005 - j0.0037 \end{bmatrix}$
4:	$\mathbf{r}_k = \mathbf{r}_k - \mathbf{Q}_k\left(\mathbf{P}_k^{\mathrm{T}}\mathbf{r}_k\right)$ (*twice*)	$\mathbf{r}_1 = \mathbf{s}_1 = \begin{bmatrix} -0.0030 - j0.0013 \\ 0.0050 + j0.0021 \\ -0.0020 - j0.0008 \end{bmatrix}$	$\mathbf{r}_2 = \begin{bmatrix} 0.0004 - j0.0014 \\ 0.0001 - j0.0002 \\ -0.0005 + j0.0016 \end{bmatrix}$
5:	$\mathbf{s}_k = \mathbf{s}_k - \mathbf{P}_k\left(\mathbf{Q}_k^{\mathrm{T}}\mathbf{s}_k\right)$ (*twice*)		$\mathbf{s}_2 = \begin{bmatrix} -0.0007 - j0.0012 \\ -0.0001 - j0.0002 \\ 0.0008 + j0.0014 \end{bmatrix}$
6:	*calculate/update* $\mathbf{T}_k$ *with* α_k, β_{k-1} *and* γ_{k-1}	$\mathbf{T}_1 = [0.052 + j0.23]$ $(\nexists\beta_0, \gamma_0)$	$\mathbf{T}_2 = \begin{bmatrix} 0.052 + j0.23 & 0.005 + j0.005 \\ 0.0067 & 0.0053 + j0.02 \end{bmatrix}$
7:	*compute the Ritz values* $\sigma^{(k)}$*, i.e., the eigenvalues* $\mathbf{\Lambda}_{T_k}$	$\mathbf{\Lambda}_{T_1} = [0.052 + j0.23]$	$\mathbf{\Lambda}_{T_2} = [0.052 + j0.23\ \ 0.0051 + j0.02]^{\mathrm{T}}$
8:	***if*** $\epsilon^{(k)} = \left\lvert\sigma^{(k)} - \sigma^{(k-1)}\right\rvert / \left\lvert\sigma^{(k-1)}\right\rvert < \Sigma$ $\rightarrow$ ***break***	$\epsilon^{(1)} > \Sigma$ $(\sigma^{(0)} = \mathrm{realmax})$	$\epsilon^{(2)} < \Sigma$ $\rightarrow$ ***break***
9:	$\beta_k = \lVert\mathbf{r}_k\rVert_2$, $\gamma_k = \mathbf{s}_k^{\mathrm{T}}\mathbf{r}_k / \beta_k$	$\beta_1 = 0.0067$, $\gamma_1 = 0.0047 + j0.0047$	–
10:	$\mathbf{q}_{k+1} = \mathbf{r}_k / \beta_k$, $\mathbf{p}_{k+1} = \mathbf{s}_k / \gamma_k$	$\mathbf{q}_2 = \begin{bmatrix} -0.45 - j0.19 \\ 0.75 + j0.31 \\ -0.30 - j0.12 \end{bmatrix}$, $\mathbf{p}_2 = \begin{bmatrix} -0.45 + j0.18 \\ 0.75 - j0.31 \\ -0.30 + j0.13 \end{bmatrix}$	–
11:	$\mathbf{Q}_{k+1} = [\mathbf{Q}_k, \mathbf{q}_{k+1}]$, $\mathbf{P}_{k+1} = [\mathbf{P}_k, \mathbf{p}_{k+1}]$	$\mathbf{Q}_2 = \begin{bmatrix} 0.577 & -0.45 - j0.19 \\ 0.577 & 0.75 + j0.31 \\ 0.577 & -0.30 - j0.12 \end{bmatrix}$, $\mathbf{P}_2 = \begin{bmatrix} 0.577 & -0.45 + j0.18 \\ 0.577 & 0.75 - j0.31 \\ 0.577 & -0.30 + j0.13 \end{bmatrix}$	–
12:	***end for***	–	***end***
13:	*compute the right eigenvectors* $\mathbf{V}_{T_k}$ *of* $\mathbf{T}_k$	–	$\mathbf{V}_{T_2} = \begin{bmatrix} 1 + j0 & -0.026 + j0.017 \\ 0.0067 - j0.03 & 1 + j0 \end{bmatrix}$
14:	*compute the Ritz vectors* $\mathbf{V}_k = \mathbf{Q}_k\mathbf{V}_{T_k}$ *and* $\mathbf{W}_k = \mathbf{P}_k\left(\mathbf{V}_{T_k}^{-1}\right)^{\mathrm{T}}$	–	$\mathbf{V}_2 = \begin{bmatrix} 0.57 + j0.012 & -0.46 - j0.18 \\ 0.59 - j0.021 & 0.73 + j0.32 \\ 0.57 + j0.0083 & -0.32 - j0.11 \end{bmatrix}$, $\mathbf{W}_2 = \begin{bmatrix} 0.57 + j0.013 & -0.46 + j0.20 \\ 0.59 - j0.020 & 0.75 - j0.29 \\ 0.57 + j0.0088 & -0.30 + j0.15 \end{bmatrix}$

where finally the $\mathbf{\Lambda}_{\mathbf{Y_B},\,100\,\mathrm{Hz}}$ eigenvalue with minimum modulus is: $\lambda_{n,f} = 1 / \mu_{k,f} + d = 1 / (0.052 + j0.23) + 0 = 0.93 - j4.13$.

VII. Conclusion

The paper presents an L_RMA approach for characterising resonances and stability issues across any poorly damped frequency range within large multi-terminal transmission grids. It is based on the non-Hermitian Lanczos method, which improves convergence time of PI-based methods for large multi-terminal transmission grids with sparse admittance matrices while maintaining accuracy. This approach can also be used to determine PFs and study the impact of power system buses on resonances, and for stability assessment in the presence of power electronics-based components. The non-Hermitian Lanczos method is a complex technique derived from the *Krylov subspaces* projection methods, and its application to RMA is not trivial. Integrating RMA with the non-Hermitian Lanczos method in the L_RMA approach posed several challenges. The performances of the new approach (L_RMA) and of RMA, r_RMA and f_RMA, are compared in ten IEEE and seven synthetic test power systems. It is concluded that r_RMA and f_RMA are generally the best options for small transmission grids, whereas L_RMA is a successful approach for large transmission grids. The sparsity ratio of the grid admittance matrix is proposed as a criterion for distinguishing between small and large transmission grids. Based on the results, an RMA-based methodology for resonance studies is proposed. This methodology can determine resonances efficiently, study the influence of grid buses on resonance using PFs, and assess small-signal stability by the PMD stability criterion. It must be highlighted that the integration of black-box models into the proposed methodology is feasible by the frequency domain characterisation of the admittance matrix. The studies in this paper are validated by MATSIM simulation. In further research, it would be interesting to compare the computational efforts of the Arnoldi and non-Hermitian Lanczos methods in detail. However, this is out of the scope of this paper.

Appendix

A numerical example of the non-Hermitian Lanczos algorithm with full re-biorthogonalisation (see Table I) application to the admittance matrix of the IEEE 3-bus test power system at 100 Hz is described step by step in Table II. It should be noted that only two iterations of the algorithm are required.

References

[1] IEEE Harmonics Model and Simulation Task Force, "Modeling and simulation of the propagation of harmonics in electric power networks: Part I," *IEEE Trans. Power Del.*, vol. 11, no. 1, pp. 452–465, Jan. 1996.

[2] J. Sun et al., "Renewable energy transmission by HVDC across the continent: System challenges and opportunities," *CSEE J. Power Energy Syst.*, vol. 3, no. 4, pp. 353–364, Dec. 2017.

[3] W. Xu, Z. Huang, Y. Cui, and H. Wang, "Harmonic resonance mode analysis," *IEEE Trans. Power Del.*, vol. 20, no. 2, pp. 1182–1190, Apr. 2005.

[4] L. Orellana, L. Sainz, E. Prieto-Araujo, M. Cheah-Mané, and O. Gomis-Bellmunt, "Study of black-box models and participation factors for the positive-mode-damping stability criterion," *Int. J. Elect. Power Energy Syst.*, vol. 148, pp. 1–10, Jun. 2023.

[5] Z. Huang, Y. Cui, and W. Xu, "Application of modal sensitivity for power system harmonic resonance analysis," *IEEE Trans. Power Del.*, vol. 22, no. 1, pp. 222–231, Feb. 2007.

[6] Y. Cui and X. Wang, "Modal frequency sensitivity for power system harmonic resonance analysis," *IEEE Trans. Power Del.*, vol. 27, no. 2, pp. 1010–1017, Apr. 2012.

[7] L. Orellana, L. Sainz, E. Prieto-Araujo, and O. Gomis-Bellmunt, "Stability assessment for multi-infeed grid-connected VSCs modeled in the admittance matrix form," *IEEE Trans. Circuits Syst. I: Reg. Papers*, vol. 68, no. 9, pp. 3758–3771, Sep. 2021.

[8] E. Ebrahimzadeh, F. Blaabjerg, X. Wang, and C. L. Bak, "Bus participation factor analysis for harmonic instability in power electronics based power systems," *IEEE Trans. Power Electron.*, vol. 33, no. 12, pp. 10341–10351, Dec. 2018.

[9] Y. Zhan, X. Xie, H. Liu, H. Liu, and Y. Li, "Frequency-domain modal analysis of the oscillatory stability of power systems with high-penetration renewables," *IEEE Trans. Sustain. Energy*, vol. 10, no. 3, pp. 1534–1543, Jul. 2019.

[10] D. Yang and Y. Sun, "SISO impedance-based stability analysis for system-level small-signal stability assessment of large-scale power electronics-dominated power systems," *IEEE Trans. Sustain. Energy*, vol. 13, no. 1, pp. 537–550, Jan. 2022.

[11] A. Quarteroni and F. Saleri, "Scientific computing with MATLAB and octave," in *Texts in Computational Science Engineering*, 2nd ed. Berlin, Germany: Springer, 2006.

[12] J. W. Demmel, *Applied Numerical Linear Algebra*. Philadelphia, PA, USA: Society for Industrial and Applied Mathematics, 1997.

[13] G. H. Golub and C. F. Van Loan, *Matrix Computations*, 3rd ed. Baltimore, MD, USA: The Johns Hopkins Univ. Press, 1996.

[14] Z. Li, H. Hu, Y. Zhou, and Z. He, "A rapid modal analysis method for harmonic resonance using modified power iteration," *IEEE Trans. Power Del.*, vol. 33, no. 3, pp. 1495–1497, Jun. 2018.

[15] Z. Li, H. Hu, Y. Wang, L. Tang, Z. He, and S. Gao, "Probabilistic harmonic resonance assessment considering power system uncertainties," *IEEE Trans. Power Del.*, vol. 33, no. 6, pp. 2989–2998, Dec. 2018.

[16] O. Cartiel, J. J. Mesas, L. Sainz, and A. Fabregas, "A faster resonance mode analysis approach based on a modified shifted-inverse power iteration method," *IEEE Trans. Power Del.*, vol. 38, no. 6, pp. 4145–4156, Dec. 2023.

[17] Y. Saad, *Numerical Methods for Large Eigenvalue Problems*. Philadelphia, PA, USA: SIAM, 2011.

[18] D. Day, "An efficient implementation of the nonsymmetric lanczos algorithm," *SIAM J. Matrix Anal. Appl.*, vol. 18, no. 3, pp. 566–589, 1997.

[19] J. Cullum, "Arnoldi versus nonsymmetric Lanczos algorithms for solving matrix eigenvalue problems," *BIT Numer. Math.*, vol. 36, no. 3, pp. 470–493, 1996.

[20] L. N. Trefethen and D. Bau, *Numerical Linear Algebra*. Philadelphia, PA, USA: SIAM, 1997.

[21] Z. Bai, J. Demmel, J. Dongarra, A. Ruhe, and H. van der Vorst, Eds., *Templates For the Solution of Algebraic Eigenvalue Problems: A Practical Guide*. Philadelphia, PA, USA: SIAM, 2000.

[22] R. B. Lehoucq, D. C. Sorensen, and C. Yang, *ARPACK Users' Guide*. Philadelphia, PA, USA: Society for Industrial and Applied Mathematics, 1998.

[23] Z. Bai, D. Day, and Q. Ye, "ABLE: An adaptive block lanczos method for non-hermitian eigenvalue problems," *SIAM J. Matrix Anal. Appl.*, vol. 20, no. 4, pp. 1060–1082, 1999.

[24] R. Itiki, M. Manjrekar, and S. G. Di Santo, "Comparative evaluation of super grid topologies proposed for Europe and Latin America," in *Proc. IEEE 51st North Amer. Power Symp.*, Wichita, KS, USA, Oct. 2019, pp. 1–6.

[25] R. Itiki, M. Manjrekar, S. G. Di Santo, and L. F. M. Machado, "Topology design method for super grids based on experiences in China and North America," in *Proc. IEEE Power Energy Soc. Innov. Smart Grid Technol. Conf.*, WA, DC, USA, Feb. 2020, pp. 1–5.

[26] R. Haydock and D. Weaire, "Computational advantages of the recursion and Lanczos methods," *Comput. Phys. Commun.*, vol. 31, no. 4, pp. 431–432, Mar. 1984.

[27] F. Gonzalez-Longatt, M. N. Acosta, M. Andrade, E. Vazquez, H. R. Chamorro, and V. K. Sood, "Multi-core platform of admittance matrix formation of power systems: Computational time assessment," in *Proc. 2020 IEEE Electric Power Energy Conf.*, Edmonton, AB, Canada, 2020, pp. 1–6.

[28] J. C. Das, *Power System Analysis: Short-Circuit Load Flow and Harmonics*, 2nd ed. Boca Raton, FL, USA: CRC Press, 2012.

[29] K. M. Sambarapu and S. M. Halpin, "Sparse matrix techniques in power systems," in *Proc. IEEE 39th Southeastern Symp. System Theory*, Macon, GA, USA, Mar. 2007, pp. 194–198.

[30] A. B. Ogundare, "Application of sparsity characteristics of power systems to AC power-flow modelling and simulation," *Int. J. Eng. Res. Technol.*, vol. 2, no. 2, pp. 1–5, Feb. 2013.
[31] H. Abaali, T. Talbi, and R. Skouri, "Comparison of Newton Raphson and Gauss Seidel methods for power flow analysis," *Int. J. Energy Power Eng.*, vol. 12, no. 9, pp. 627–633, 2018.
[32] S. Parvathy, K. C. Sindhu, and T. N. Padmanabhan, "Response of voltage source model of UPFC in an IEEE 5 bus system for power flow enhancement," in *Proc. IEEE Int. Conf. Technological Advancements Power Energy*, 2017, pp. 1–5.
[33] A. Al-Hinai, "Voltage collapse prediction for interconnected power systems," Master Thesis, West Virginia Univ., 2000.
[34] R. Abu-Hashim et al., "Test systems for harmonics modelling and simulation," *IEEE Trans. Power Del.*, vol. 14, no. 2, pp. 579–587, Apr. 1999.
[35] "IEEE 24-bus system," Electric Grid Test Case Repository. Accessed: Oct. 14, 2023. [Online]. Available: https://electricgrids.engr.tamu.edu/electric-grid-test-cases/ieee-24-bus-system/
[36] M. Shahidehpour and Y. Wang, *Communication and Control in Electric Power Systems: Applications of Parallel and Distributed Processing. Appendix C*. Hoboken, NJ, USA: Wiley, Jun. 2003.
[37] T. Athay, R. Podmore, and S. Virmani, "A practical method for the direct analysis of transient stability," *IEEE Trans. Power App. Syst.*, vol. PAS-98, no. 2, pp. 573–584, Mar. 1979.
[38] R. Christie, "57 bus power flow test case," Power System Test Archive, Aug. 1993, Accessed: Oct. 14, 2023. [Online]. Available: https://labs.ece.uw.edu/pstca/pf57/pg_tca57bus.htm
[39] R. Christie, "118 bus power flow test case," Power System Test Archive. 1993, Accessed: Oct. 14, 2023. [Online]. Available: https://labs.ece.uw.edu/pstca/pf118/pg_tca118bus.htm
[40] R. Christie, "300 bus power flow test case," Power Systems Test Case Archive. Aug. 1993, Accessed: Oct. 14, 2023. [Online]. Available: https://labs.ece.uw.edu/pstca/pf300/pg_tca300bus.htm
[41] "Illinois 200-bus system: ACTIVSg200," Electric Grid Test Case Repository. Accessed: Oct. 14, 2023. [Online]. Available: https://electricgrids.engr.tamu.edu/electric-grid-test-cases/activsg200/
[42] "South carolina 500-bus system: ACTIVSg500," Electric Grid Test Case Repository. Accessed: Oct. 14, 2023. [Online]. Available: https://electricgrids.engr.tamu.edu/electric-grid-test-cases/activsg500/
[43] A. B. Birchfield, T. Xu, K. M. Gegner, K. S. Shetye, and T. J. Overbye, "Grid structural characteristics as validation criteria for synthetic networks," *IEEE Trans. Power Syst.*, vol. 32, no. 4, pp. 3258–3265, Jul. 2017.
[44] "Texas synthetic grid –6716 buses," Electric Grid Test Case Repository. Accessed: Oct. 14, 2023. [Online]. Available: https://electricgrids.engr.tamu.edu/texas7k/
[45] "ACTIVSg70k: 70,000 bus synthetic grid on footprint of Eastern United States," Electric Grid Test Case Repository. Accessed: Oct. 14, 2023. [Online]. Available: https://electricgrids.engr.tamu.edu/electric-grid-test-cases/activsg70k/
[46] N. Hatziargyriou et al., "Definition and classification of power system stability – revisited & extended," *IEEE Trans. Power Syst.*, vol. 36, no. 4, pp. 3271–3281, Jul. 2021.